# Bacteriostatic, silver-doped, zirconia-based thin coatings for temporary fixation devices tuning stem cells' expression of adhesion-relevant genes and proteins

Biomaterials Advances 176 (2025) 214360

Contents lists available at ScienceDirect

Biomaterials Advances

journal homepage: www.journals.elsevier.com/materials-science-and-engineering-c

# Bacteriostatic, silver-doped, zirconia-based thin coatings for temporary fixation devices tuning stem cells' expression of adhesion-relevant genes and proteins

Sara Ferraris [a], Alessandro C. Scalia [b], Mauro Nascimben [b], Sergio Perero [a], Lia Rimondini [b], Silvia Spriano [a,*], Andrea Cochis [b]

[a] Department of Applied Science and Technology, Politecnico di Torino, Italy
[b] Department of Health Sciences, Center for Translational Research on Autoimmune and Allergic Diseases CAAD, Università del Piemonte Orientale UPO, Italy

ARTICLE INFO

*Keywords:*
Antiadhesion
Antibacterial
Coatings
Temporary fixation devices
OMICS

ABSTRACT

Temporary fixation devices must support bone healing, be easily removed without bone tissue overgrowth, and reduce the risk of infection. To match these needs, mechanically and chemically stable thin coatings, based on a zirconia matrix doped with silver (ZrO2-Ag), were sputtered on Ti6Al4V. Coatings with two silver concentrations were produced: a low (0.2 % at Ag) concentration (AL) for bacteriostatic effect and a high (0.5 % at Ag) concentration (AH) for antibacterial properties. Surfaces were characterized for silver content and release, mechanical adhesion, morphology, roughness, wettability, and surface zeta potential, reporting high stability and a continuous Ag release over 28 days. Direct cytocompatibility was shown for human mesenchymal stem cells (hMSC), while antibacterial properties were verified towards *Staphylococcus aureus*. Results revealed non-toxic and anti-adhesion effects of AL that were deeply investigated towards hMSC by a multi-omics approach. Transcriptomics revealed a down-regulation of cadherins- and integrins-related genes involved in the cell-to-cell and cell-to-substrate adhesion, whereas proteomics confirmed a reduced expression of adhesion proteins (Talin and Ras homolog family member A - RhoA). The OMICS profiles were matched by bioinformatics analysis, confirming a cluster of preserved biological functions strongly related to the cells' adhesion but not to apoptosis. Therefore, AL is a good candidate for bone temporary fixation devices, not interfering with bone healing (cytocompatible), avoiding bone adhesion on the implant surface, and being bacteriostatic.

## 1. Introduction

It is widely accepted that the surface properties of biomaterials have a significant role in cellular and bacterial adhesion to implants [1]. However, while the research of innovative pro-regenerative and antibacterial surfaces is extremely active especially in the field of permanent implants [2,3] few works can be reported focused on the peculiar needs of temporary implants: those devices are usually applied for a short period to stabilize fractures during the initial management of polytrauma patients, but then they are removed in order to proceed with the definitive treatment [4]. Their primary purpose is not to induce or enhance osteogenesis, but rather to stabilize the bone. As such, materials designed for temporary fixation devices should not support cell adhesion or proliferation (as permanent implants), since their removal prior to prosthesis implantation could damage the bone if tissue ingrowth occurs [5]; nevertheless, materials must still be cytocompatible to prevent the release of toxic compounds in the healing site. The main issues associated with temporary fixation devices are bacterial contamination and tissue overgrowth. Bacterial colonization can lead to the development of a severe infection requiring antibiotic therapies or even device removal in the worst scenario. Undesired tissue overgrowth can make surgical removal of the device very complex, with the risk of causing fractures [6–8].

To overcome these issues, some literature underlines the role of surface roughness on tissue adhesion, thus suggesting for the development of extremely smooth surfaces to prevent tissue overgrowth on temporary fixation devices [9,10]. Moreover, it can be speculated that surface roughness is a key factor influencing bacterial adhesion, too. In fact, a threshold of Ra for microbial adhesion has frequently been reported in the literature to be set at 0.2 μm to avoid the presence of

* Corresponding author.
*E-mail address:* silvia.spriano@polito.it (S. Spriano).

https://doi.org/10.1016/j.bioadv.2025.214360
Received 31 March 2025; Received in revised form 22 May 2025; Accepted 26 May 2025
Available online 27 May 2025

anchorage points for the pathogens' adhesion [11,12].

Beyond roughness control, other literature deals with the development of innovative coatings based on functionalization with silica and ornidazole [13], chitosan and hyaluronic acid [14], or vitamin E [15], to cite some examples. Nowadays, only a temporary fixation device with a biodegradable coating releasing the antibiotic Gentamicin (Depuy Synthes PROtect™), and two devices with coatings/surface treatments releasing silver ions (Agluna® Accentus and LOQTEQ® antibacterial AAP Implantate AG) are available on the market.

In this context, the Authors previously reported the development of thin inorganic coatings of potential interest for temporary fixation devices based on silica, alumina, or zirconia, doped with silver, with very smooth topography, being able to reduce bacterial adhesion [16]. Based on these previous results, in the present work, the zirconia matrix was selected due to its better stability in physiological conditions and was enriched with different amounts of silver (Ag) to obtain surfaces able to match different clinical needs: (i) infection prevention at the early stage by low-Ag (named AL) and (ii) infection treatment in a high-risk situation by high-Ag (named AH). Ag is widely employed in antibacterial coatings for its well-known ability to eradicate bacteria by disrupting membrane integrity, protein synthesis, DNA replication, or by causing oxidative stress by the production of reactive oxygen species (ROS) within the cytoplasm [17]. However, its unpredictable behaviour poses risks to eukaryotic cells, necessitating the use of a concentration toxic to bacteria yet safe for cells; in fact, as recently reported by the Authors, a good balance between antibacterial properties and cytocompatibility is not easy to find [18]. Moreover, cytocompatibility must be maintained, but direct cells' colonization on temporary devices should be discouraged to prevent undesired tissue overgrowth.

Based on these premises, AL and AH $ZrO_2$-Ag coatings were characterized for their physical-chemical properties through silver content and release, adhesion, morphology, roughness, wettability, and surface zeta potential. Then, biological characterization was focused on cytocompatibility towards human mesenchymal stem cells (hMSC) and antibacterial efficacy to counteract *Staphylococcus aureus* infection. AL specimens reported promising non-toxic anti-adhesive properties; so hMSC cultivated onto such specimens were deeply investigated by transcriptomics and proteomics, investigating for an eventual effect, due to released Ag, modulating the expression of genes and proteins involved in cell-to-cell and cell-to-substrate adhesion. Finally, bioinformatics analysis was exploited to reveal the biological functions influenced by the AL coatings and highly preserved from RNA to protein expression.

## 2. Materials and methods

### 2.1. Specimens' physical-chemical characterization

#### 2.1.1. Specimens' preparation

Ti6Al4V samples (10 mm × 20 mm × 2 mm) were sectioned using electro-discharge machining. The material was identified as compliant with ASTM B348 specification for Grade 5 titanium alloy, exhibiting the following chemical composition (in wt%): Al = 5.50–6.75; V = 3.5–4.5; Fe <0.4; O < 0.2; C < 0.08 %; H 0.01; N 0.05; Ti: balance; tot impurities <0.4. Samples were mirror polished (abrasive papers up to P4000 and diamond paste of 1 μm) and washed in an ultrasonic bath, once in ethanol, 5 min, and two times in ultrapure water, 10 min each. Thin films constituted of a zirconia matrix, enriched with silver, were deposited by means of the co-sputtering technique [16]. A custom-designed Kenosistec™ three confocal sputtering equipment was used. In particular, pure (99.9 % $ZrO_2$, NanoVision™) and pure (99.99 % Ag, NanoVision™) targets were used on two confocal 3 in. circular cathodes, both magnetron-type. On the $ZrO_2$ cathode, radio frequency (RF) power was supplied, while for Ag DC was used. The depositions were performed in pure Ar atmosphere at 5.5 dPa (5.5 μbar) pressure, while pre-deposition pressure was 1 μPa ($10^{-5}$ mbar). Two different concentrations of silver were considered: (i) low Ag concentration (Ag content around 0.2%at, named as AL specimens) for bacteriostatic surfaces aimed at preventing surface infection, and (ii) Ag high concentration (Ag content around 0.5%at, named AH specimens) for antibacterial surfaces aimed at killing bacteria colonies on the surface. Undoped zirconia coatings (named Z specimens) and Ti6Al4V (Ti) substrate were considered as a control.

#### 2.1.2. Surface characterizations

Coating adhesion resistance to mechanical stress was evaluated by means of the tape and scratch tests. The tape test was performed according to the Standard Test Methods for Rating Adhesion by Tape Test (ASTM D 3359, Standard test methods for measuring adhesion by tape test) [19].

The scratch test was performed on a CSM Revetest equipped with a Rockwell tip with a radius of 200 μm. Three scratches were done on each sample with a linear applied load of 1–20 N, a scratching rate of 10 mm/min, and a length of 2 mm. Two critical loads (Lc) were determined based on the photo analysis of the scratch. The first failure, Lc1, corresponds to initial cracking, the second failure, Lc2, to partial delamination of the coating from the substrate. For each coating, the full trace and an example of the two critical loads are shown.

Surface roughness (Ra) was measured by a contact surface profiler equipped with a diamond stylus tip (Talysurf Intra Touch Ultra™, from Taylor Hobson, UK).

Then, the coating chemical stability and the release of characteristic elements (Ag and Zr) were investigated by soaking 3 samples per type in 25 ml of ultrapure water at 37 °C up to 28 days. As a comparison, a similar release test was also performed in PBS (phosphate-buffered saline 79,382-50TAB Sigma Aldrich) at 37 °C for samples Z and AH (3 specimens per type). The release medium was completely changed at each time point. Surface composition before (day 0) and after soaking (day 28) was determined by means of Energy Dispersive Spectroscopy (EDS, JEOL, JED 2300™). Ion release was quantified by means of Inductively Coupled Plasma (ICP-MS; iCAP™ Q spectrometer, Thermo Fisher Scientific, Waltham, MA, USA).

Zeta potential titration curves were obtained with an electrokinetic analyzer (SurPASS, Anton Paar™) equipped with an adjustable gap cell. A pair of samples was inserted in the cell with a gap (≅ 100 μm) between them. 0.001 M KCl was used as an electrolyte and forced to flow in the gap. The streaming potential was measured and zeta potential was obtained by the instrument software (Attract). The electrolyte pH was 5.5 at the beginning of each measure, then it was titrated with 0.05 M HCl down to pH 2 (acid range). The samples and the instrument were then washed with ultrapure water and new KCl electrolyte was prepared (pH 5.5). A basic titration was obtained by the progressive addition of 0.05 M NaOH up to 9 (basic range) with the automatic titration unit of the instrument.

### 2.2. Biological characterization

#### 2.2.1. Antibacterial properties

Specimens' ability to prevent surface bacterial colonization was verified towards the commercial MRSA strain *Staphylococcus aureus* (ATCC 43300, from the American Type Culture Collection). Bacteria were cultivated at 37 °C overnight in Luria Bertani broth (LB, from Sigma, Milan); then, the bacteria suspension was diluted 1:10 in LB and incubated again at 37 °C for 3 h to achieve the logarithmic growth phase. Before each test, bacteria were diluted in fresh medium in order to reach a final concentration of $1 \times 10^5$ cells/ml corresponding to an optical density of 0.001 at 590 nm wavelength. Specimens were directly infected onto the surface by drop-seeding a defined number of bacteria ($1 \times 10^3$ cells/specimen) and incubated at 37 °C. After 2, 4, and 24 h from the infection, the supernatant was gently removed from the specimens' surface, avoiding enzymes. At each time-point, the viability of surface-adhered bacteria was evaluated as their metabolic activity by

the colorimetric assay Alamar blue (ready-to-use kit from Life Technologies, Milan) using a spectrophotometer (Tecan Spark, Tecan, USA) at 590 nm wavelength fluorescence. The number of non-adhered floating bacteria was obtained by the Colonies Forming Units (CFUs) assay [20]. The viability was visually confirmed using the Live/dead fluorescent assay (BacLight from Life Technologies, Milan) by confocal microscopy (Leica TCS SP8 LIGHTNING, from Leica Systems, Basel). To rank the Z, AL and AH specimens' activity, bulk Ti6Al4V specimens were used as a positive control; experiments were performed using triplicate.

#### 2.2.2. Cytocompatibility evaluation

To verify specimens' in vitro cytocompatibility, commercial human bone marrow-derived mesenchymal stem cells (hMSC, PromoCell C-12974) were exploited as a model of the tissue self-healing process. Cells were maintained in DMEM Low glucose supplemented with 15 % Fetal Bovine serum (FBS, from Sigma) and 1 % antibiotics (penicillin/streptomycin). After reaching 70–80 % confluence, cells were detached by trypsin-EDTA solution, harvested and used for experiments. Cells were directly drop-wise seeded onto the specimens' surface ($3{,}5 \times 10^3$ cells/specimen) and incubated at 37 °C, 5 % $CO_2$ for cultivation. Afterwards, the viability of the surface-adhered cells was evaluated by the Alamar blue metabolic assay as previously described; moreover, non-adhered cells in the supernatant were collected, counted by trypan blue into a Bürker chamber and then spotted into a new 24-multiwell plate for 24 h after that their viability was visually checked by the Live/dead assay (L/D from Life Technologies, Milan) by fluorescent microscopy (EvosFLoid, from Invitrogen, Milan). To rank the Z, AL and AH specimens' cytocompatibility, bulk Ti6Al4V specimens were used as positive control; experiments were performed using triplicate.

### 2.3. OMICS profiling

#### 2.3.1. Transcriptomics by RNAseq

To determine the anti-adhesion or pro-apoptotic effect due to the Ag doping, the genetic profile of cells cultivated directly onto the surface of the specimens was screened by total RNA sequencing (RNA-seq). Accordingly, after 24 h of cultivation, floating cells were collected from the supernatants and the total RNA was extracted and analyzed with an Illumina 550 NexSeq sequencer for their coding and non-coding regions. RNA was isolated using miRNeasy Tissue/Cells Advanced Mini Kit (Qiagen, Hilden, Germany); RNA concentration was measured using QubitTM RNA BR Assay Kit on a QubitTM 4.0 Fluorometer (Invitrogen, Thermo Fisher Scientific Inc.) while its integrity was assessed using an Agilent 4200 TapeStation System with the Agilent High Sensitivity RNA ScreenTape Assay (both from Agilent Technologies Inc., Santa Clara, CA, USA). All RNA samples showed an RNA integrity number (RIN) $\geq 9$ and were considered high-quality samples. For mRNA-seq library preparation, 300 ng of total RNA per sample was captured using oligo(dT) magnetic beads-based protocol using the Illumina® Stranded mRNA Prep, Ligation Kit (Illumina Inc., San Diego, CA, USA). Libraries were sequenced on an Illumina NextSeq™ 550 platform (Illumina Inc.) using a NextSeq 500/550 High Output Kit v2.5 (150 cycles, $2 \times 75$ bp read length, paired-end) (Illumina Inc.) to achieve sufficient read depth for the bioinformatics analysis. Finally, for bioinformatics analysis, Fastq files were trimmed using Trimmomatic [21] with the option SLIDINGWINDOW on the entire sequence length to keep only reads with an average Phred quality >30. Good quality reads were used in input for the RSEM software pipeline [22] to quantify expressed genes, using STAR [23] as aligner and hg38 as reference genome. Gene annotation was obtained from Ensembl v100. Data matrix containing expressed genes were filtered to keep only the genes with TPM > 2 in at least one sample. DESeq2 [24] was used to evaluate differentially expressed genes. Lists of "adhesion" genes were selected using Gene Ontology annotation downloaded by Ensembl Biomart, selecting all the genes associated with the keyword "adhesion" in the Gene Name, GO Term accession, GO term name or GO term definition. Venn diagrams were produced using InteractiVenn [25]. Heatmaps were produced using "pheatmap" package in R. Functional analysis was performed with ToppGene (Bonferroni test, significance set at $p < 0.01$).

#### 2.3.2. Proteomics

To confirm whether the direct contact with the specimens' surface modified the cells' protein expression as well as their genetic profile, total DNA was extracted from adhered and floating cells, and the proteomic profile was obtained by mass spectrometry using a Q Exactive Plus Mass Spectrometer (from Thermo Scientific, Milan). Cells were collected, washed, lysed with RIPA buffer, and sonicated. Proteins were then precipitated with cold acetone and resuspended. Proteins were then reduced in 25 μL of 100 mM $NH_4HCO_3$ with 2.5 μL of 200 mM DTT (Merck) at 60 °C for 45 min and next alkylated with 10 μL 200 mM iodoacetamide (Merck) for 1 h at RT in dark conditions. The iodoacetamide excess was removed by adding 200 mM DTT. Proteins were digested with trypsin. The digests were dried by Speed Vacuum and then desalted. Digested peptides were analyzed with a UHPLC Vanquish system (Thermo Scientific, Milan) coupled with an Orbitrap Q-Exactive Plus (Thermo Scientific, Milan). Peptides were separated by a reverse phase column (Accucore™ RP-MS 100 × 2.1 mm, particle size 2.6 μm). The column was maintained at a constant temperature of 40 °C at a flow rate of 0.200 ml/min. Mobile phase A and B were water and acetonitrile respectively, both acidified with 0.1 % formic acid. The analysis was performed using the following gradient: 0–5 min from 2 % to 5 % B; 5–55 min from 5 % to 30 % B; 55–61 from 30 % to 90 % B and hold for one minute, at 62.1 min the percentage of B was set to the initial condition of the run at 2 % and hold for about 8 min to re-equilibrate the column, for a total run time of 70 min. The mass spectrometry analysis was performed in positive ion mode. The ESI source was used with a voltage of 2.8 kV. The capillary temperature, sheath gas flow, auxiliary gas, and spare gas flow were set at 325 °C, 45 arb, 10 arb, and 2, respectively. S-lens was set at 70 rf. For the acquisition of spectra, a data-dependent (ddMS2) top-10 scan mode was used. Survey full-scan MS spectra (mass range $m/z$ 381 to 1581) were acquired with resolution R = 70,000 and AGC target $3 \times 106$. MS/MS fragmentation was performed using high-energy c-trap dissociation (HCD) with resolution R = 35,000 and AGC target $1 \times 106$. The normalized collision energy (NCE) was set to 30. The injection volume was 3 μL. The mass spectra analysis was carried out using MaxQuant software (version 1.6.14). MaxQuant parameters were set as follow: trypsin was selected for enzyme specificity; the search parameters were fixed to an initial precursor ion tolerance of 10 ppm and MS/MS tolerance at 20 ppm; as fixed modification, carbamidomethylation was set, whereas oxidation was set as variable modification. The maximum missed cleavages were set to 2. Andromeda search engine searched the spectra in MaxQuant against the Uniprot_CP_Human_2018 sequence database. Label-free quantification was performed, including a match between runs option with the following parameters: protein and peptide false discovery rate was set to 0.01; the quantification was based on the extracted ion chromatograms, with a minimum ratio count of 1; the minimum required peptide length was set to 7 amino acids. Proteomics data generated from the mass spectrometry were analyzed through the MetaboAnalyst software; the functional analysis of the regulated proteins was done through the STRING software.

### 2.4. Bioinformatic analysis of the similarity between OMICS profiles

To gain additional insights on how proteomic and transcriptomic expression levels interplay, they were analyzed as single entities with an ad hoc procedure rather than through correlation. Indeed, in theory, higher mRNA expression levels should result in higher protein expression since proteins are translated from mRNA; however, the correlation between mRNA and protein levels might not be perfect due to post-transcriptional regulation factors, different translational control between genes, post-translational modifications, and the dependence of

correlation on the specific tissue type, cell line, or experimental conditions (i.e., stress response). For these reasons, the analysis of shared regulatory factors was conceptualized as a distance-based mapping between proteins and genes over a Cartesian plane (Fig. 1a).

The procedure aims at evaluating which genes are activated by the low silver concentration coating (AL) compared to bare titanium (Ti cnt), jointly using proteomics and transcriptomics expression levels. Considering titanium as the baseline condition, modifications on gene expression data activated by AL could be measured using distance metrics to summarize the degree of relationship and interpret changes connected to biological modifications on both transcriptomic and proteomic data. Cosine distance could represent the coherence between transcriptomic and proteomic findings, whereas the Euclidean distance should reflect expression level changes in the two experimental conditions (schematized in Fig. 1b). The proposed workflow started, excluding proteins or gene expression levels with missing values. The initial number of proteins was 590 (5 excluded), whereas the initial genes were 60,683, lowered to 27,050 due to the inconsistencies in the data. Afterwards, the raw values from the three cell lines were log-transformed for the proteomic and transcriptomic datasets, and z-score standardization was performed.

### 2.5. Statistical analysis of data

For the biological characterization, experiments were performed using three replicates. Normal distribution and homoscedasticity were tested with Wilk–Shapiro's and Levene's tests, respectively. Samples were statistically compared by the statistical package for the social sciences (SPSS) software (v25, IBM, New York, NY, USA) using the one-way ANOVA test and Tukey's post-hoc analysis. Results were considered significant for $p < 0.05$. For the OMICS assays, statistical analyses are detailed in the specific sub-chapters 2.3.1 and 2.3.2, respectively.

## 3. Results and discussion

### 3.1. Surfaces' physical-chemical properties

The visual appearance of the samples immediately after the coating is shown in Fig. 2a, upper panel. Visually, the zirconia coating (Z) appeared to be mostly golden when undoped, violet when doped with low silver content (AL), and close to blue when doped with high silver content (AH). In the clinical scenario, the observed colors can allow fast and easy identification of the coating typologies, which have different potential applications: anti-adhesive (AL) or antibacterial (AH). Z is used in this paper mainly as a reference for a coating without silver doping. It has potential as a protective ceramic coating on Ti6Al4V to improve surface chemical stability, hardness, and tribological properties [26], but this aspect was not investigated in this paper.

The tape and scratch tests were performed to measure the coatings' mechanical stability: results are reported in Fig. 2b–c. Both the low (AL) and high silver (AH) content coatings registered an optimal adhesion to the Ti6Al4V substrate: in fact, both AL and AH specimens were ranked as 5B (corresponding to 0 % detachment) according to guidelines of the tape test (ASTM D 3359).

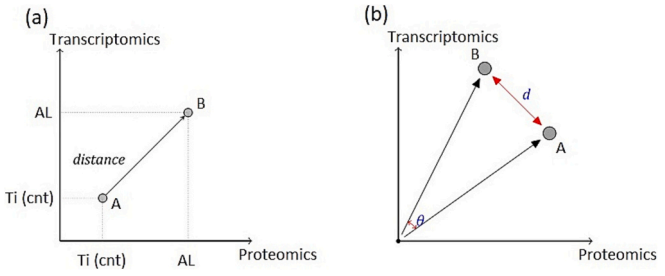


**Fig. 1.** (a) Conceptualization of Ti (cnt) and AL averaged samples analysis employing mutually proteomics and transcriptomic expression profiles. (b) Visual interpretation of Euclidean (d) and cosine (θ) metrics for each experimental pair of points.

Concerning the scratch test, the registered critical loads were: Lc1(Z) = 6.2 ± 1.4; Lc2(Z) = 9.6 ± 0.07; Lc1 (AL) = 5.2 ± 0.4; Lc2 (AL) = 9.7 ± 0.8; Lc1 (AH) = 5.9 ± 0.79; Lc2 (AH) = 11.9 ± 1.97. No significant differences were observed between the undoped $ZrO_2$ coating (Z) and that with a low Ag content (AL), while a slightly higher second critical load was found for the sample doped with a high Ag content (AH), indicating a higher adhesion of the coating. As far as the type of cracks is concerned (Fig. 2c), there were no substantial differences between the three coatings. The scratch tracks of the coatings exhibited brittle chipping at lower loads and severe spallation at high loads. For both critical loads, cracks were mainly noticed at the edges of the tracks. The observed scratch resistances are in agreement with previous data obtained by the authors. A brittle behaviour is expected for a ceramic coating and concerning the quantitative values obtained for the scratch resistance, they are comparable to those reported for a chemically treated titanium surface finalized to permanent implants (Lc1 = 4–5 N; Lc2 = 9 N) [27], which was demonstrated to survive without evident damages to a simulated implantation in an animal bone [28].

Surface roughness was then measured to understand how the coating deposition changed micro-roughness; results demonstrated that Z, AL, and AH specimens hold a Ra value between 0.10 μm and 0.13 μm, comparable to the Ti6Al4V substrate. Moreover, such micro-roughness can be considered acceptable for biomedical applications because the literature states that the threshold of Ra to not favor bacterial adhesion is 0.2 μm [12,29].

Subsequently, the release of characteristic elements (Ag and Zr) was investigated over 28 days by soaking specimens in water. The initial colors did not substantially change after soaking, as reported in Fig. 2a, lower panel. This observation can be interpreted as macroscopic evidence of the chemical stability of the coating towards environmental degradation. The chemical surface composition was compared by EDS analysis before (day 0) and after (day 28) the soaking; results are reported in Fig. 3. As expected, the silver release (Fig. 3a) was proportional to the silver content in the coating (lower for the AL samples and higher for the AH ones). AL was designed to reduce the risk of infection by a bacteriostatic action on the implant surface, while AH was designed to be actively antibacterial by killing bacteria in the surrounding area of the implant [16]. In both cases, the total amount of the released ions was lower than the threshold for cytotoxicity reported in the literature for silver ions (LD50 (Ag) ≅ 0.4 mg/l) [30]. Moreover, even if an early release boost was registered in the first days, a continuous further Ag emission was observed for all the tested 28 days, thus suggesting a constant reservoir of active principle preventing secondary infections after surgery. The zirconium release (Fig. 3b), which is associated with an eventual matrix degradation, was extremely low for the whole soaking period and can be considered negligible; this evidences the zirconia matrix chemical stability, confirming the lack of significant degradation over the tested 28 days. Results of the ionic release (concerning Ag and Zr) were confirmed by a test in an inorganic solution (PBS - phosphate-buffered saline) closer to the physiological fluids (S1), confirming that the presence of inorganic salts does not affect the results.

As a confirmation, EDS analysis (Fig. 3c) showed that the surface composition was almost constant before (day 0) and after 28 days of soaking; the only exception is represented by a certain reduction of the Ag content, as previously demonstrated. The stability of the zirconia-based coatings agreed with previous results reported by the Authors dealing with similar coatings compared with others based on alumina- and silica [16].

Finally, the zeta potential titration curves of the bare Ti6Al4V substrate and the coated samples (Z, AL, and AH) were investigated; results are reported in Fig. 4. The Ti6Al4V substrate showed an isoelectric point

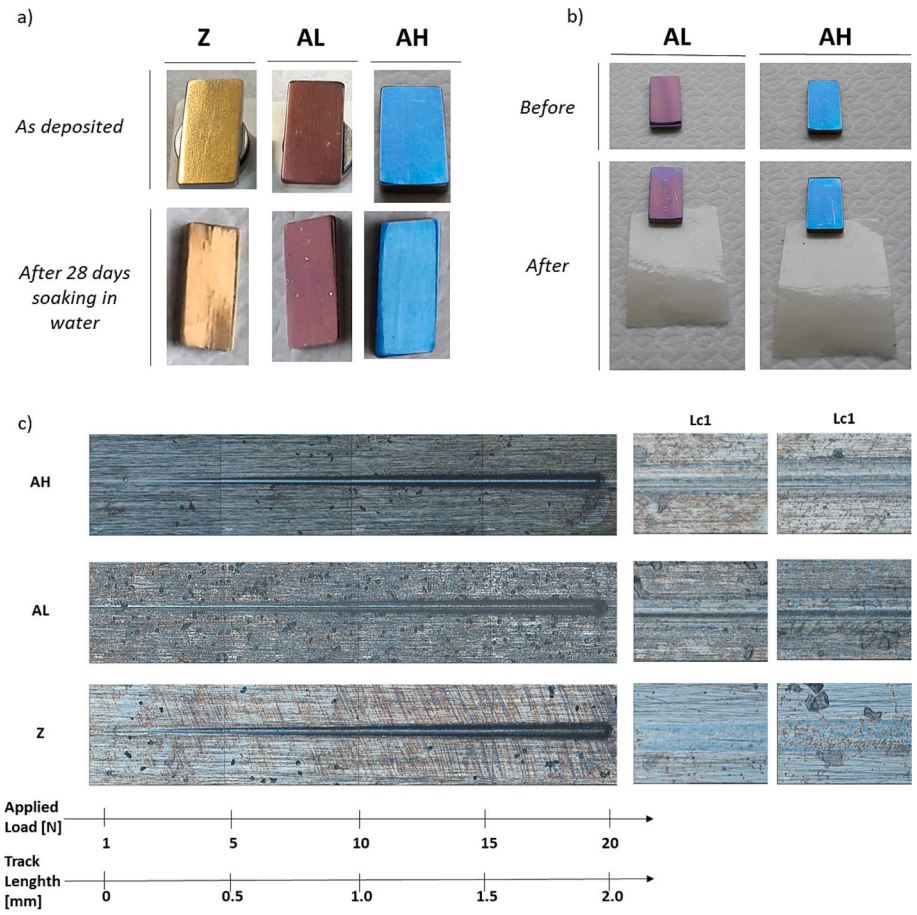


**Fig. 2.** Soaking and tape test. (a) Visual appearance of coated samples before and after 28 days soaking in ultrapure water. The colors were maintained thus demonstrating stability over time. (b) Tape test images demonstrated an optimal adhesion of the coatings as almost no detachment was observed after the test. (c) Images of the scratches performed on the different samples and enlargements of the areas corresponding to the critical loads (Lc1–Lc2).

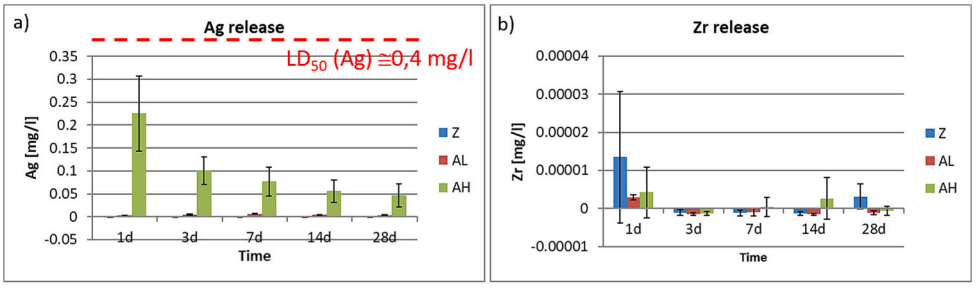


c)

| | Z | | AL | | AH | |
|---|---|---|---|---|---|---|
| | Before | After | Before | After | Before | After |
| O | 43.91±3.00 | 42.86±2.07 | 48.19±1.71 | 49.59±1.85 | 53.87±1.05 | 53.58±0.80 |
| Al | 5.30±0.22 | 5.57±0.42 | 4.96±0.38 | 5.11±0.40 | 4.41±0.21 | 4.34±0.14 |
| Ti | 49.78±2,87 | 50.66±1.71 | 45.45±1.23 | 44.05±1.57 | 39.10±0.88 | 39.61±0.63 |
| Zr | 0.92±0.16 | 0.86±0.08 | 1.21±0.20 | 1.01±0.49 | 2.08±0.11 | 2.05±0.16 |
| Ag | 0.12±0.07 | 0.06±0.07 | 0.20±0.03 | 0.08±0.08 | 0.54±0.04 | 0.43±0.11 |

**Fig. 3.** Ion release and surface composition studies. (a) Silver was constantly released over 28 days in quantities correlated with the starting composition (AH or AL), but always in a smaller quantity than LD50 (indicated by the red line). (b) Conversely, Zr was almost not released, demonstrating the coating stability that was confirmed by the EDS results (c) where no significant differences were observed in terms of surface composition before (day 0) and after soaking (day 28). Bars and values represent means±dev.st. of n = 3 replicates. (For interpretation of the references to color in this figure legend, the reader is referred to the web version of this article.)

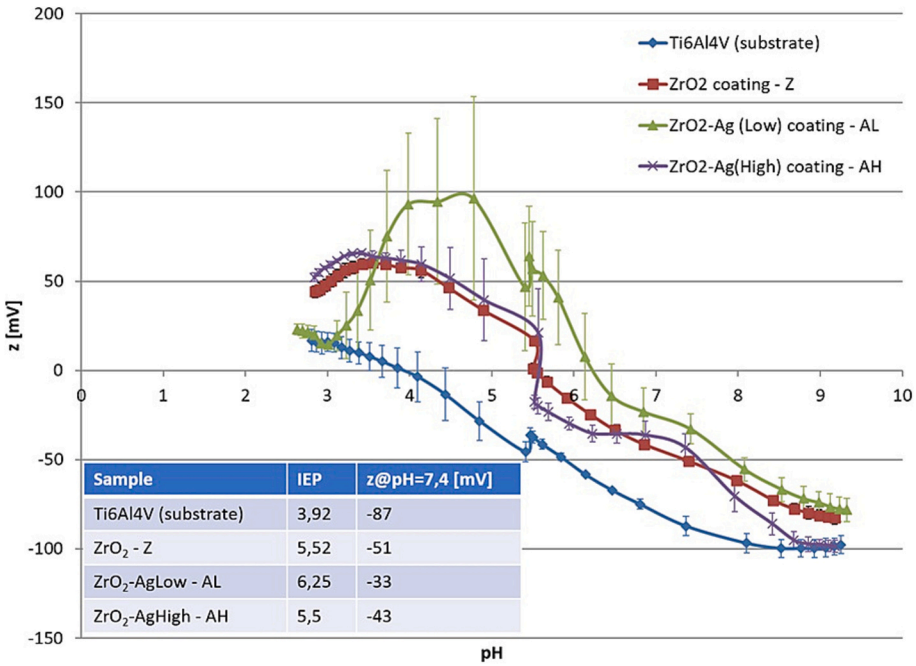


| Sample | IEP | z@pH=7,4 [mV] |
|---|---|---|
| Ti6Al4V (substrate) | 3,92 | -87 |
| $ZrO_2$ - Z | 5,52 | -51 |
| $ZrO_2$-AgLow - AL | 6,25 | -33 |
| $ZrO_2$-AgHigh - AH | 5,5 | -43 |

**Fig. 4.** Zeta potential. Specimens' titration curves reported an isoelectric point (IEP) close to 4 for bulk Ti specimens, while zirconia-based coatings (Z, AL and AH) evidenced IEPs at more basic values (5.50–6.25).

(IEP) close to 4; this is typical of surfaces lacking specific functional groups with an acid-basic reactivity, in accordance with previous literature dealing with bulk titanium surfaces [31,32]. According to the detected IEP value, the Ti6Al4V surface can be considered as negatively charged at physiological buffered pH (7.4), and no plateaus were detected in the curve. This represents a plausible finding because the presence of a plateau is usually related to the exposition of functional groups, which are completely deprotonated/protonated above/below a specific pH value in contact with an aqueous solution. The zirconia-based coatings (Z, AL and AH) evidenced IEPs at more basic values in comparison to Ti6Al4V (5.50–6.25). The detected IEPs are close to what was previously reported by the Authors for similar $ZrO_2$-Ag coatings deposited on stainless steel [16], but significantly higher than the IEP previously obtained on specimens of bulk zirconia [33]. However, different properties of thin film coatings with respect to the bulk materials are not surprising and are worth investigating. The zeta potential of the Zr-based coatings resulted in a negative value at physiological pH (as usual for implant biomaterials), but positive at the inflammatory one (pH 4–5), thus suggesting an interesting acid-basic reactivity of these surfaces in pro-inflammatory conditions. In fact, a positive zeta potential at pro-inflammatory acidic pH can induce an interesting "smart" mechanism of the material to counteract bacterial adhesion and biofilm formation when the increase of the infection causes an acidification of the environmental pH [34]. A moderate plateau in the acid region can also be associated with the exposition of functional groups (likely Ti-OH groups) with a basic reactivity, in agreement with the shift of the IEPs towards a higher value of pH, compared to the Ti substrate. The standard deviations of zeta potential registered for the Ag-doped coatings are significantly larger with respect to the undoped zirconia one (almost negligible). This is explainable considering the high chemical stability of the undoped coating in contrast with the silver release by the doped ones.

### 3.2. Specimens biological characterization

#### 3.2.1. Antibacterial properties

One of the major drawbacks of titanium and its alloys (such as Ti6Al4V) is represented by the ease with which bacteria colonize their surface; unfortunately, as reported by very recent literature dealing with clinical revisions of orthopedic implants [35], infections still represents a primary cause of implant failure despite the large research done to confer antibacterial properties to implantable materials. Here, silver (Ag) was selected as a potential antibacterial agent due to its broad-spectrum activity targeting both Gram+ and Gram- strains due to the different killing mechanisms, which hardly allow bacteria to develop effective resistance mechanisms [17]. Regarding the target strain, *Staphylococcus aureus* was selected due to its frequent involvement in orthopedic medical device infection [36]; bacteria were forced to adhere to the specimens' surface by an established protocol from the Authors [37] to simulate the device colonization. Antibacterial properties of the undoped (Z) and Ag-doped (AL and AH) zirconia coatings were ranked considering Ti as a control.

As expected, results of surface-adhered bacteria metabolic activity (Fig. 5a) demonstrated an increasing activity over time of the Ti control and undoped Z specimens; on the opposite, Ag doping determined a significant reduction for both AL and AH specimens in comparison to Ti and Z starting to 4 h of direct contact (Fig. 5a, $p < 0.05$ indicated by # and §). The reduction of metabolically active pathogens was considered as a parameter for the % of viable bacteria that were normalized towards Ti (=100 %); results revealed a reduction of ~45 % for AL and 78 % for AH after 12 h (Fig. 5b, $p < 0.05$ indicated by # and § in comparison to Ti and Z, respectively). These results were logically correlated to the amount of surface-deposited Ag by hypothesizing a dose-dependent effect. However, we also analyzed the number of viable floating bacteria released in the supernatant due to detachment from the specimens' surface by colonies forming unit (CFU), as well as with fluorescent live/dead staining, and unexpected results were observed, as reported in Fig. 5c, d, and e. The number of viable bacteria in the supernatant of the AL samples after 24 h was comparable to the Ti and Z ones CFU count (Fig. 5c), which disagrees with the metabolic activity results. Results from live/dead staining (Fig. 5d), followed by dot count by ImageJ software (Fig. 5e), were coherent with each other and confirmed the presence of a numerous viable (stained in green) bacterial population of the AL supernatant. On the opposite, results from AH supernatants were aligned with the metabolic activity ones, reporting the presence of a statistically significant lower number of viable bacteria in comparison to

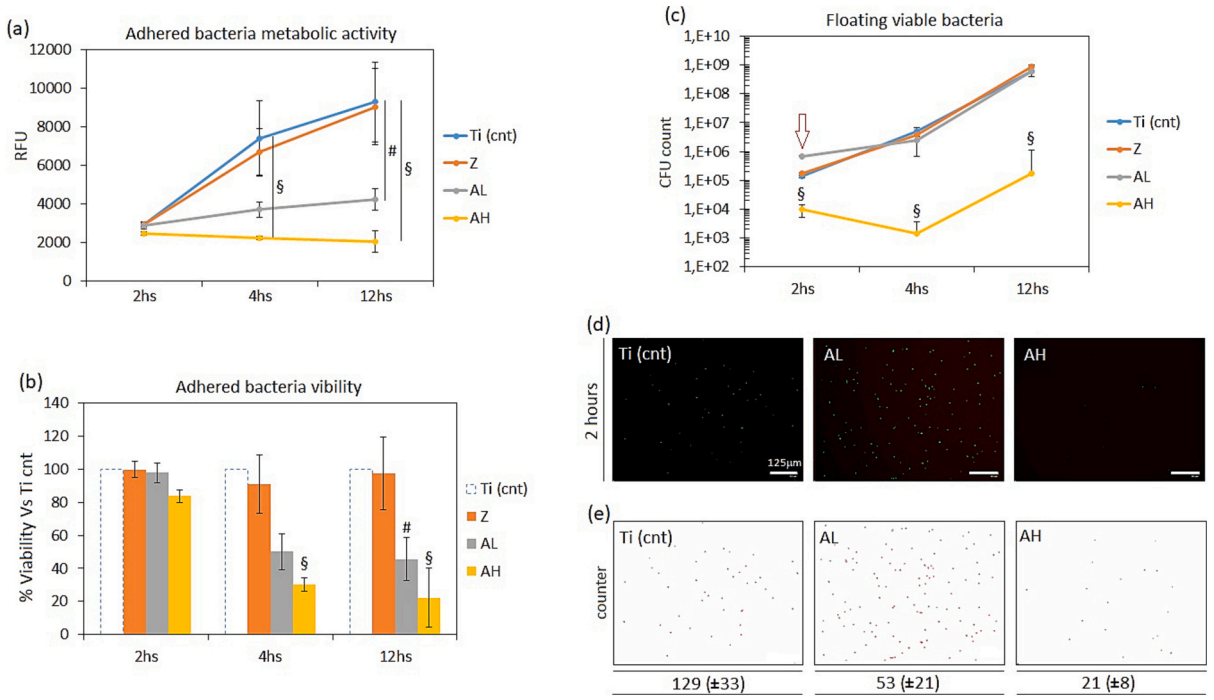


**Fig. 5.** Antibacterial properties. (a) The metabolic activity of adhered bacteria was significantly reduced by the Ag doping of AL and AH specimens in comparison to Ti ($p < 0.05$, indicated by §) and Z ($p < 0.05$, indicated by #), (b) bringing to a viability reduction of ~45 % for AL and ~ 78 % for AH in respect to Ti after 12 h. However, (c) the CFU count of floating surface-detached bacteria reported a comparable number of viable bacteria for Ti and Z. AL displayed a higher, though not statistically significant, increase in bacterial count, while AH resulted in significant reduction ($p < 0.05$, indicated by §). (d) Fluorescent live/dead images, based on SYTO9 and Propidium Iodide staining, confirmed CFU results and (e) the dots count done by ImageJ software showed the representative number of bacteria/fields. Bars and lines represent means±dev.st of n = 3 replicates.

Ti, Z, and AL as coherently demonstrated by CFU count (Fig. 5c, $p < 0.05$ indicated by §), live/dead staining (Fig. 5d) and dots count (Fig. 5e). So, we hypothesized that the Ag amount on AH was, actually, effective in eradicating bacteria by contact-killing effect, whereas the Ag amount on AL was mostly anti-adhesion rather than antibacterial, thus preventing surface colonization but not providing a significant killing effect.

### 3.2.2. *Cytocompatibility*

As previously discussed in the introduction, a good balance between antibacterial and cells' friendly Ag surface doping is not an easy-to-solve matter. Even if the LD50 of silver ions is generally defined by literature to be around 0.4 mg/l [30,38], the release profile and the possible interactions with other chemicals from the coating can influence the different stages of cells' colonization, from early adhesion and spread to proliferation. Accordingly, we seeded human mesenchymal stem cells (hMSC) directly onto the surface of the specimens for 24 h to evaluate cell behaviour. hMSCs were selected due to their common use as a representative in vitro model of cells deputed for tissue healing.

Results of hMSC metabolic activity initially suggested a dose-dependent toxicity due to silver; in fact, values were significantly lower for AL and AH when compared to Ti or Z (Fig. 6a, $p < 0.05$ indicated by # and §, respectively). As a consequence, the viability obtained by the normalization of metabolic activity results towards Ti (= 100 %), suggesting a reduction of 66 % for AL and 75 % for AH of viable cells colonizing specimens' surface (Fig. 6b).

However, taken in consideration the anti-adhesion effect previously observed for the AL specimens in the antibacterial assays (previously reported in Fig. 5), we collected the supernatants covering the specimens seeded with cells, counted the number of viable detached cells by trypan blue and Bürker chamber and moved them to a new polystyrene plate to confirm their ability to adhere, spread and proliferate into a new substrate as a confirmation of their metabolic activity. Very interestingly, a large number of viable cells (around 42 % of the seeded ones, Fig. 6c, $p < 0.05$ indicated by #) was found to be detached in the supernatants of AL specimens, thus confirming the hypothesis that such substrates hold intrinsic anti-adhesion properties rather than a toxic effect as previously observed for the antibacterial essays. On the opposite, the detached cells from AH specimens were almost all dead, thus confirming that the Ag amount loaded into those specimens is in fact in a range of high toxicity even for eukaryotic cells. Accordingly, the low number of detached cells from Ti and Z can probably be justified by the evidence that the majority of cells correctly adhered to the surface, as demonstrated by the high metabolic activity in Fig. 6a. As a further confirmation, when detached cells were moved to a new polystyrene plate for 24 h (Fig. 6d) and then marked by fluorescent live/dead assay (Fig. 6e) AL reported >95 % of viable cells (stained in green) while AH showed a > 97 % of dead cells (marked in red). Therefore, in line with previous findings of the antibacterial assay we hypothesized that the AL surfaced did not produce a real toxic effect on hMSC, but rather avoided cell adhesion in the first colonization step. On the opposite, AH surfaces prevented specimens' colonization by imposing a toxic effect.

In conclusion, a promising anti-adhesion effect was observed for the AL specimens in view of a potential application for temporary devices: cells are not stimulated to adhere by a non-toxic surface composition thus preventing the formation of tissue overgrowth but without introducing cytotoxicity. This result corresponds exactly to the clinical need to use, for a short period, a cytocompatible material able to support the fixation of the bone but not to allow its growth to avoid damaging the tissue at the time of removal.

## 3.3. *OMICS profiling*

The results obtained by the cytocompatibility and antibacterial studies suggested an interesting anti-adhesion and non-toxic effect of the AL specimens towards cells and bacteria. This can be of great interest for a possible clinical application of temporary implants due to the

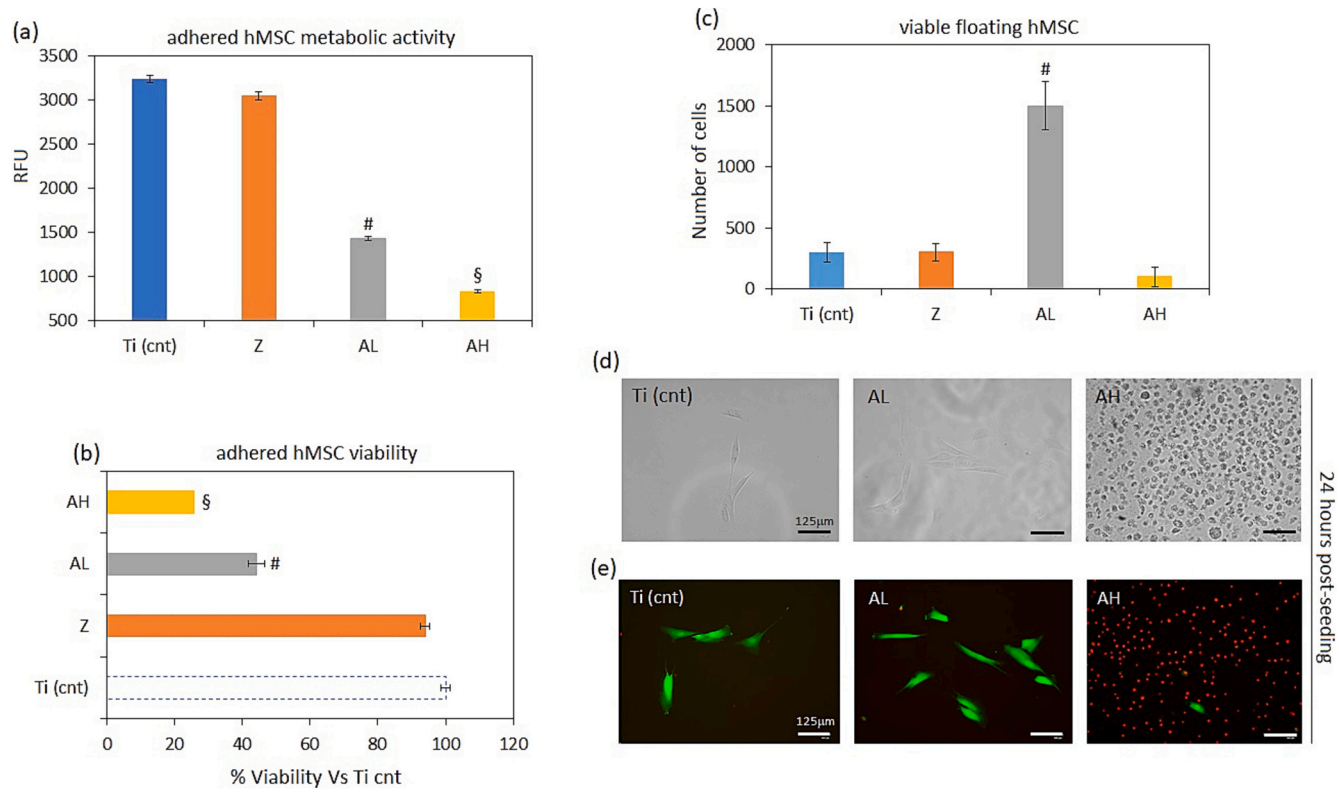


**Fig. 6.** Cytocompatibility. (a–b) Cells' metabolic activity and viability were significantly reduced by the Ag doping of both AL and AH in respect to Ti and Z ones ($p < 0.05$, indicated by # and §, respectively); (c) however, by counting the number of viable cells detached from specimens, a large number (~42 %) was observed for AL thus suggesting for an anti-adhesion effect rather than a toxic one. This non-toxic anti-adhesive effect was confirmed by morphology (d) and live/dead staining of detached cells (e) that showed >95 % of viable cells (calcein-positive stained green) for AL after being cultivated into a new substrate. Bars represent means±dev.st of n = 3 replicates. (For interpretation of the references to color in this figure legend, the reader is referred to the web version of this article.)

possibility of preventing infections and, at the same time, tissue overgrowth on the device that will be soon removed without causing cytotoxic side effects to the healing tissue. To confirm whether the observed anti-adhesion effect was due to the surface properties, human mesenchymal stem cells (hMSC) cultivated in direct contact with AL specimens were analyzed for their transcriptome by RNAseq and compared to the bulk Ti ones to unravel the regulated genes. Then, proteomics was applied to verify whether the influence of the specimens towards cells' genome was transduced into comparable protein regulation and to confirm the transcriptome regulation. The bulk Ti was considered as control due to the evidence that the transcriptome of hMSC cultivated on this substrate was comparable (> 97 % match) to the ones cultivated on the gold standard polystyrene, as reported in Supplementary (S2) 1.

### 3.3.1. *Transcriptomics studies*

The comparison of the transcriptome of cells cultivated on control (Ti) and AL test specimens revealed 811 differentially expressed genes (DEGs). In line with the hypothesis of the anti-adhesion role of the surface functionalization, 71 genes have been categorized by the Gene Ontology annotation (by Ensembl Biomart) as "*adhesion genes*". The generated heatmap showing the difference in gene expression between AL and Ti specimens is presented in Fig. 7a, where downregulated and upregulated genes are distinguished by blue and red colors, respectively (AL vs Ti).

Then, the functional analysis of the regulated genes was performed with ToppGene (by Bonferroni test, a threshold set at $p < 0.01$) to correlate detected genes with the respective biological processes, cellular components, or molecular functions. As a result, in Fig. 7b, the obtained terms are clustered into downregulated genes (green), upregulated genes (red), and miscellaneous genes (blue), respectively. Very interestingly, "*cell adhesion*", "*cell-substrate adhesion*", and "*cell-cell adhesion*" are the most significant terms identified by the software based on the genes differently expressed on the AL samples compared to the Ti controls.

In detail, the complete lists of genes clustered in the above-mentioned biological processes are summarized in Table 1.

The surface composition of the AL specimens significantly influenced the expression of Protocadherin Beta 8 (PCDHB8), Protocadherin Beta 7 (PCDHB7), Protocadherin Beta 16 (PCDHB16), and Protocadherin Beta 13 (PCDHB13), all members of the cadherin superfamily. This group of genes is crucial for the early t cell-to-cell and cell-to-substrate adhesion phase and their functionality is strictly dependent on calcium; in this regard, Li et al. [39] demonstrated that silver ions cause depolarization of the plasma membrane by interfering with calcium and potassium exchange. So, the observed poor adhesion of cells cultivated on AL specimens can actually be hypothesized due to the interference of Ag released from the surface. As a confirmation of this hypothesis, RNAseq revealed that AL significantly influenced the expression of Integrin Subunit Alpha 6 (ITGA6) and Integrin Subunit Alpha 2 (ITGA2), consistent with previous results obtained by Martin et al [40]

Similarly, a reduction in the expression level of collagen I and collagen III has been observed. Collagen I and III are the main structural elements of the extracellular matrix, providing tensile strength, supporting migration, and regulating cell adhesion [41]. Although a direct effect of silver ions on the downregulation of these specific genes has not been observed before, there is a large literature describing the role of silver in reducing cell membrane stability [42–44], supporting our findings.

Taken together these results, the simultaneous downregulation of genes involved in cell adhesion and the upregulation of genes involved in cadherin binding can appear to be contradictory; however, the genes involved in cadherin bindings are mainly chromatin condensation genes

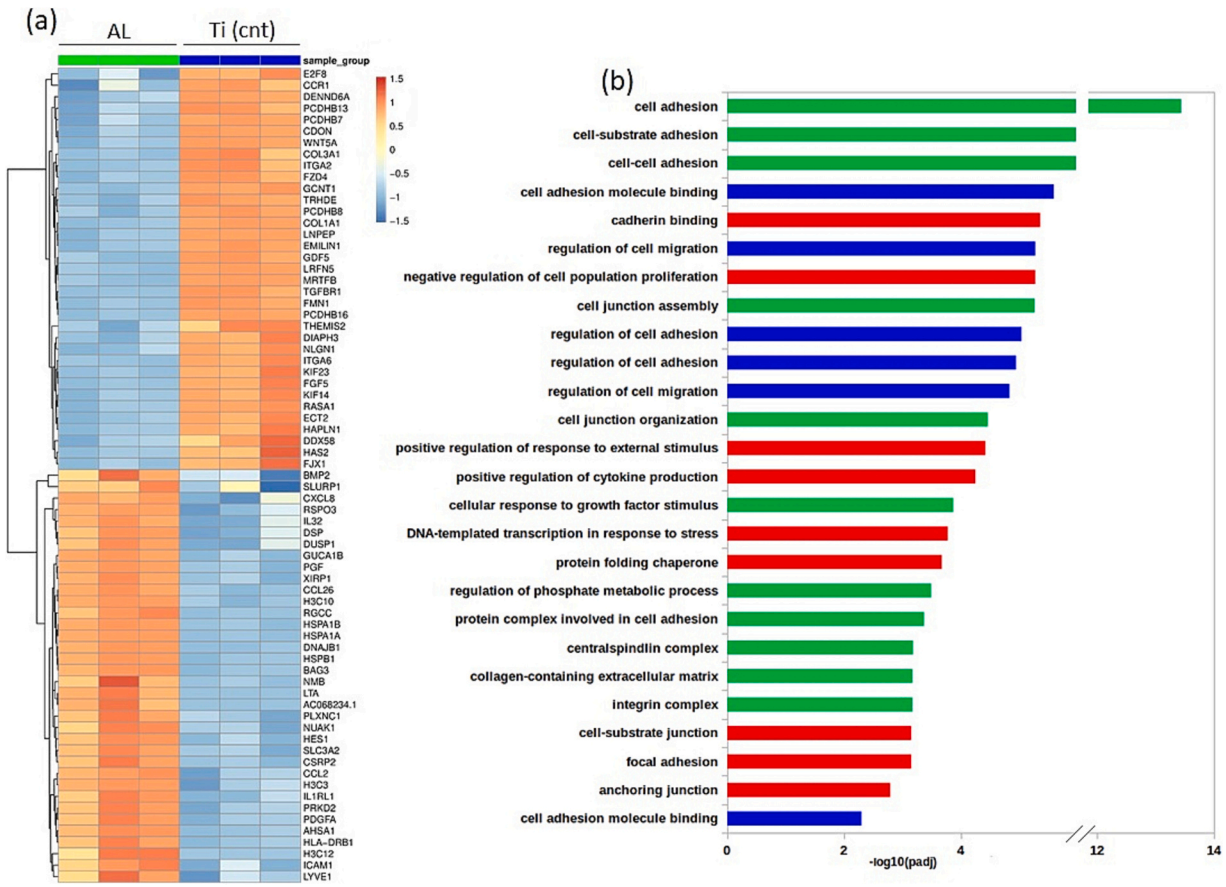


**Fig. 7.** Transcriptomics studies by RNAseq. (a) Heatmap of differentially expressed genes (DEGs) upregulated (red) and downregulated (blue) in hMSC cultivated in direct contact with AL or Ti specimens. (b) Functional analysis of the biological processes upregulated (red), downregulated (green) and miscellaneous (blue) according to the detected genes. This analysis confirmed that the observed anti-adhesion effect reported by the AL specimens is due to the down-regulation of genes responsible for to the biological processes identified as "cell adhesion", "cell-substrate adhesion", and "cell-cell adhesion". (For interpretation of the references to color in this figure legend, the reader is referred to the web version of this article.)

**Table 1**
Lists of genes clustered into specific biological functions identified by the functional analysis.

| Biological function | Strength (−log10 (padj)) | Genes |
|---|---|---|
| Cell adhesion | 13.44466367 | PCDHB8, PCDHB7, COL3A1, THEMIS2, FZD4, ITGA6, KIF14, CCR1, NLGN1, DENND6A, ITGA2, GCNT1, HAS2, RASA1, EMILIN1, FMN1, LRFN5, WNT5A, PCDHB16, CDON, PCDHB13, HAPLN1, COL1A1 |
| Cell-substrate adhesion | 6.20999648 | COL3A1, FZD4, ITGA6, KIF14, ITGA2, HAS2, RASA1, EMILIN1, FMN1, COL1A1 |
| Cell-cell adhesion | 6.20999648 | PCDHB8, PCDHB7, ITGA6, NLGN1, DENND6A, ITGA2, GCNT1, HAS2, EMILIN1, LRFN5, WNT5A, PCDHB16, CDON, PCDHB13 |

(H3C3, H3C10, and H3C12) or genes involved in the upregulation of HSPs (DNAJB1, AHSA1, HSPA1A, and BAG3). The upregulation of H3 Clustered Histone 3 (H3C3), H3 Clustered Histone 10 (H3C10), and H3 Clustered Histone 12 (H3C12) causes chromatin condensation, a phenomenon often associated with a condition of stress that Morais et al. [42] correlated to the presence of silver as the leading agent causing this unfavourable condition. Therefore, previous literature was again helpful to support and justify our findings.

### 3.3.2. *Proteomics profile*

The volcano plot in Fig. 8a displays the 552 unregulated proteins (in grey), the 20 downregulated proteins (in blue, AL vs Ti), and the 13 upregulated proteins (in red, AL vs Ti). Six out of 33 have been categorized as proteins involved in focal adhesion by GeneOntology. Fig. 8b reports, among these six, the upregulated and downregulated proteins in green and red, respectively. The upregulated proteins include members of the Heat Shock Protein (HSP) family, such as HSP family A member 1B (HSPA1B), HSP family A member 5 (HSPA5), and HSP family A member 8 (HSPA8). Discovered in the early 1960s, HSPs were initially associated with heat shock responses; however, recent literature reported their expression during tissue remodeling or after exposure to metal ions [45]. Notably, the upregulated HSPs belong to the heat shock 70 superfamily (Hsp70s) and play the role of chaperonins assisting various biological events, including protein assembly and folding [46]. Chakraborty et al. [47] demonstrated that the upregulation of this family directly impairs the stability of Talin (TLN), a key mechanosensing protein assisting cells 'adaptation and adhesion to surfaces; in line with these findings, here, TLN was found to be significantly downregulated in cells, being in contact with AL specimens. Similarly, the HSP upregulation determined a significant reduction of the Ras homolog family member A (RhoA) expression; however, similarly to TLN, this protein has been reported in the literature as playing a pivotal role in the actin rearrangement when cells adapt their cytoskeleton to the topography of the target surface [48–50]. So, further evidence of the direct role of the AL surfaces' composition in influencing the behaviour of the cells in tight contact seems to be revealed.

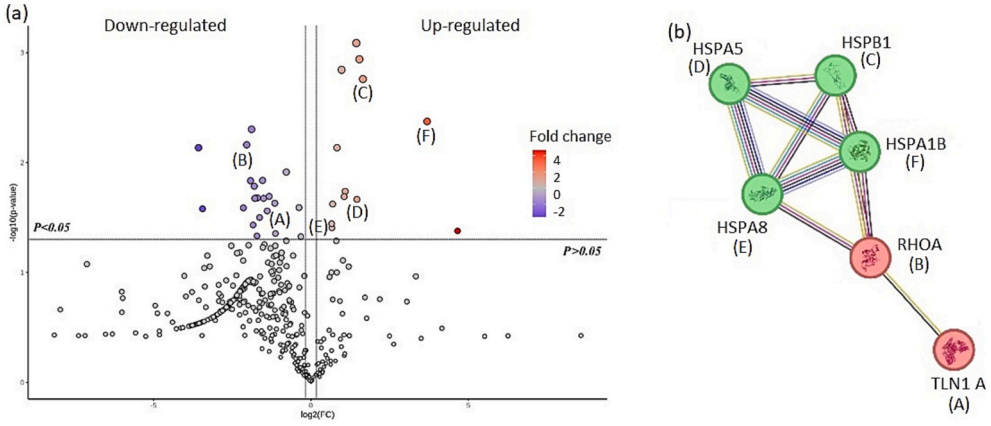


**Fig. 8.** Proteomics studies. (a) Volcano plot, where the intersection of the lines indicates the threshold of significance. Dots on the plot represent unregulated, downregulated, and upregulated proteins in grey, blue, and red, respectively. (b) Functional analysis of the regulated proteins using the STRING software. The graph depicts upregulated and downregulated proteins in green and red, respectively. (For interpretation of the references to color in this figure legend, the reader is referred to the web version of this article.)

Finally, in line with TLN and RhoA findings, proteomics reported downregulation of Galectin 3 and Eukaryotic translation initiation factor 5A-1; they are involved in cell-matrix adhesion and cell-cycle progression, respectively, thus bringing other evidences of how the AL specimens' properties directly affect the ability of cells to properly adhere to the target substrate [51]. To the best of our knowledge, a direct effect of silver ions on their downregulation has never been observed before in the literature.

### 3.4. Similarity between OMICS profiles

The relationship between transcriptomics and proteomics lies in that mRNA transcripts serve as templates for protein synthesis [52]. However, the relationship is only sometimes straightforward due to factors affecting protein abundance and post-transcription activity, such as alternative splicing, mRNA stability, translation efficiency, and post-translational modifications [53]. Accordingly, here we applied a bioinformatic approach where transcriptomics and proteomics averaged measurements evaluated by Euclidean and cosine distances to establish the degree of closeness between Ti cnt and AL experimental patterns. The intention was to quantify the dissimilarity or similarity between expression levels and data types: closer data points should have a small Euclidean distance, thus the average expression levels for Ti cnt and AL are similar, implying no difference due to AL coating, while Cosine distance could reinforce this assumption highlighting relationships or exposing peculiar patterns between transcriptomic and proteomic datasets [54]. As a result of applying the Euclidean and Cosine distances on the dataset under investigation, it was possible to obtain a scatterplot representing the analogy between the proteomics and transcriptomics data (Fig. 9a); then, the expression levels were clustered by the unsupervised algorithm DBSCAN (Density-Based Spatial Clustering of Applications with Noise) to group data points based on similarities allowing for a more focused analysis on interesting subsets. So, 3 clusters were identified (Fig. 9b) and interpreted as follows: Cluster 1 groups results showing different patterns between experimental conditions (Ti cnt Vs AL) but reporting a low match between transcriptomic and

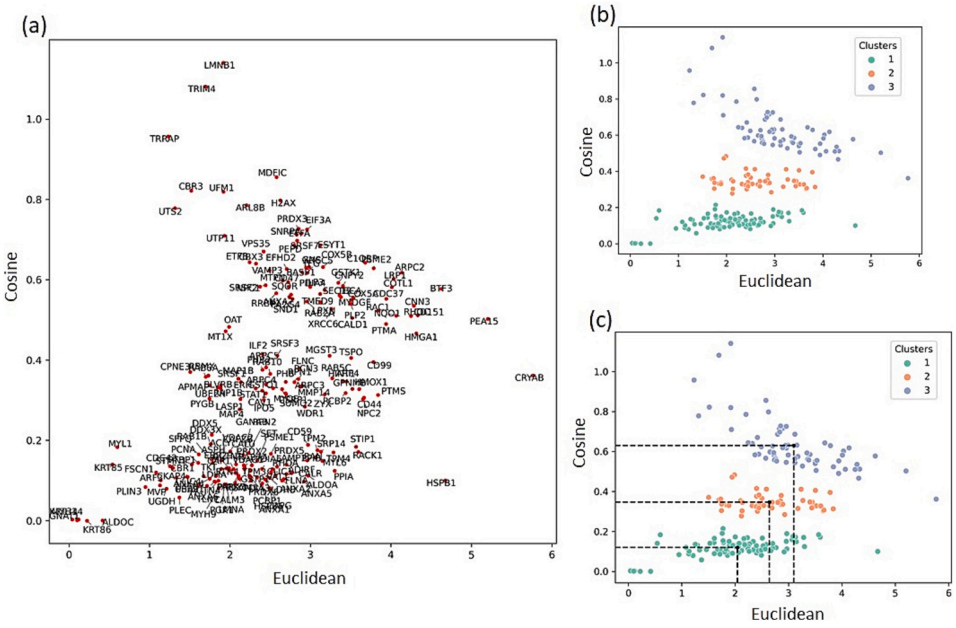


**Fig. 9.** Comparison of OMICS profiling. (a) Average distance of Ti cnt and AL specimens from proteomics and transcriptomics dataset applying the proposed procedure. (b) Groups of the genes as identified by distance metrics values. (c) Groups of the genes as identified by distance metrics values and their means: Cluster 3 contains points with major differential expression measures in the two metric values.

proteomic measurements, meaning that the profiles exhibited by the two metrics do not match completely each other. On the opposite, Cluster 3 gather data where both proteomics and transcriptomics match in revealing the pathways up-regulated by the AL coating in comparison to the Ti bulk control. Finally, Cluster 2 is in the middle of these two conditions, with moderate variations due to AL in terms of magnitude difference and mild divergence between proteomic and transcriptomic findings. Further evidence can be appreciated in Fig. 9c which highlights the centers of the three clusters aligned over an increasing trend where Cluster 3 showed a high "consensus" between transcriptomic and proteomic datasets in identifying relevant changes due to Ti (cnt) presence.

Based on the results obtained by the OMICS signatures comparison, Table 2 reports the enrichment findings on the genes belonging to Cluster 3 with all databases' searches [55,56]. The table contains the significant terms of gene ontology (GO subdivided in BP biological process, MF molecular function, and CC cellular component), signaling pathway (KEGG, Reactome, WikiPathways), regulatory motifs in DNA (TRANSFAC, miRTarBase), protein databases (Human Protein Atlas, CORUM), and human phenotype ontology. Only statistically significant databases' search results were included (p-value adjustment by Bonferroni correction).

Very interesting, the enrichment analysis revealed that proteomics and transcriptomics matched in the main biological functions previously correlated to the non-toxic anti-adhesion effect of the AL coatings; in fact, functions such as "*focal adhesion*", "*cell-substrate junction*", "*anchoring junction*", "*protein binding*", "*cytoskeletal protein binding*", "*actin binding*" clearly refer to the different ability of hMSC to adhere or detach from Ti and AL substrates. As a consequence, functions like "*cellular response to chemical stimulus*", "*response to endogenous stimulus*" are most likely activated by the direct contact of the cells with the Ag that determined a spontaneous detachment rather than pro-apoptotic pathways. Finally, the different secretory profile highlighted by the "*secretory vesicle*" and "*cytoplasmic vesicle*" suggest even for a different signaling profiles which would be very interesting to evaluate for future experiments.

## 4. Conclusions

Bacterial adhesion and bone tissue overgrowth are the main issues affecting the clinical success of trauma temporary fixation devices. The specific goal for these implants is a cytocompatible coating, not interfering with bone healing (cytocompatible), but with an anti-adhesive behaviour for bone cells, to avoid bone damage when the implant is removed, and low bacterial contamination, to reduce the risks of infection. Moreover, the coating must be chemically and mechanically stable. In the present research, Ag-doped zirconia thin films were obtained on Ti6Al4V substrates by sputtering. The proposed coatings present low roughness (around 0.1 μm, close to the substrate one), optimal mechanical adhesion (0 % detachment at tape test and good scratch resistance) and long-lasting (up to 28 days), tailorable Ag release (proportional to silver content in the coating). Zirconia films with low silver content (AL) were cytocompatible for mesenchymal stem cells but were able to reduce cellular and bacterial adhesion. For the first time, the ability of these coatings to downregulate specific adhesion-related

**Table 2**
Enrichment analysis on Cluster 3 entries (grey and white background distinguish the different sources).

| Source | Native | Name | p_value |
|---|---|---|---|
| CORUM | CORUM:27 | Arp2/3 protein complex | 1.70475E+16 |
| CORUM | CORUM:6289 | Prohibitin 2 complex, mitochondrial | 1.03322E+16 |
| CORUM | CORUM:1183 | CDC5L complex | 1.18865E+16 |
| GO:BP | GO:0070887 | Cellular response to chemical stimulus | 1.80767E+15 |
| GO:BP | GO:0009719 | Response to endogenous stimulus | 2.3083E+16 |
| GO:BP | GO:0007163 | Establishment or maintenance of cell polarity | 2.40187E+15 |
| GO:CC | GO:0005925 | Focal adhesion | 15311925.57 |
| GO:CC | GO:0030055 | Cell-substrate junction | 200558396.2 |
| GO:CC | GO:0005615 | Extracellular space | 287345306 |
| GO:CC | GO:0070161 | Anchoring junction | 870774353.5 |
| GO:CC | GO:0005576 | Extracellular region | 889978218.4 |
| GO:CC | GO:0030054 | Cell junction | 1.26547E+11 |
| GO:CC | GO:0005737 | Cytoplasm | 26504765818 |
| GO:CC | GO:0005885 | Arp2/3 protein complex | 3.91112E+15 |
| GO:CC | GO:0099503 | Secretory vesicle | 4.45954E+15 |
| GO:CC | GO:0031410 | Cytoplasmic vesicle | 2.13265E+16 |
| GO:CC | GO:0043227 | Membrane-bounded organelle | 3.35727E+15 |
| GO:CC | GO:0098588 | Bounding membrane of organelle | 3.49543E+15 |
| GO:MF | GO:0005515 | Protein binding | 1.43962E+15 |
| GO:MF | GO:0051015 | Actin filament binding | 2.49588E+16 |
| GO:MF | GO:0008092 | Cytoskeletal protein binding | 4.2302E+15 |
| GO:MF | GO:0044877 | Protein-containing complex binding | 8.46095E+15 |
| GO:MF | GO:0003779 | Actin binding | 2.04288E+15 |
| GO:MF | GO:0003925 | G protein activity | 4.36452E+15 |
| KEGG | KEGG:04144 | Endocytosis | 3.07732E+15 |
| KEGG | KEGG:05418 | Fluid shear stress and atherosclerosis | 1.52752E+16 |
| KEGG | KEGG:05100 | Bacterial invasion of epithelial cells | 1.89718E+16 |
| MIRNA | MIRNA:hsa-miR-1-3p | hsa-miR-1-3p | 1.56112E+15 |
| REAC | REAC:R-HSA-168249 | Innate immune system | 4.01392E+16 |
| REAC | REAC:R-HSA-6798695 | Neutrophil degranulation | 9.3438E+15 |
| WP | WP:WP4495 | IL 10 anti inflammatory signaling pathway | 2.72125E+15 |

genes and to reduce the adsorption of related proteins was demonstrated in the present work. The present research demonstrates that sputtered silver-doped zirconia thin films can effectively satisfy the requirements of temporary fixation devices, reducing risks associated with bacterial adhesion and tissue overgrowth. Moreover, the sputtering technique is a green, competitive and easily scalable approach suitable for the production of medical devices.

## CRediT authorship contribution statement

**Sara Ferraris:** Writing – original draft, Supervision, Methodology, Investigation, Conceptualization. **Alessandro C. Scalia:** Writing – original draft, Investigation. **Mauro Nascimben:** Writing – original draft, Software, Methodology, Investigation. **Sergio Perero:** Writing – original draft, Investigation. **Lia Rimondini:** Writing – original draft, Supervision, Conceptualization. **Silvia Spriano:** Writing – original draft, Supervision, Project administration, Methodology, Funding acquisition, Conceptualization. **Andrea Cochis:** Writing – original draft, Supervision, Methodology, Investigation, Conceptualization.

## Declaration of competing interest

The authors declare the following financial interests/personal relationships which may be considered as potential competing interests: Silvia Spriano reports financial support was provided by European Commission - local agency Finpiemonte. If there are other authors, they declare that they have no known competing financial interests or personal relationships that could have appeared to influence the work reported in this paper.

## Acknowledgements

Easy-Fix project, MANUNET call 2017 is acknowledged for funding (European Commission through the local agency Finpiemonte). Part of this activity has been done within the PolitoBIOMedLab –Biomedical Engineering Lab. INTRAUMA S.p.a is acknowledged for collaboration and helpful discussion.

## Appendix A. Supplementary data

Supplementary data to this article can be found online at https://doi.org/10.1016/j.bioadv.2025.214360.

## Data availability

No data was used for the research described in the article.

## References

[1] B. Kasemo, Biological surface science, Surf. Sci. 500 (1–3) (2002) 656–677, https://doi.org/10.1016/s0039-6028(01)01809-x.
[2] S. Spriano, S. Yamaguchi, F. Baino, S. Ferraris, A critical review of multifunctional titanium surfaces: new frontiers for improving osseointegration and host response, avoiding bacteria contamination, Acta Biomater. 79 (2018) 1–22, https://doi.org/10.1016/j.actbio.2018.08.013.
[3] J. Raphel, M. Holodniy, S.B. Goodman, S.C. Heilshorn, Multifunctional coatings to simultaneously promote osseointegration and prevent infection of orthopaedic implants, Biomaterials 84 (2016) 301–314, https://doi.org/10.1016/j.biomaterials.2016.01.016.
[4] D. Bose, D. Piper, Temporary external fixation in the management of orthopaedic trauma, Orthop. Traumatol. 35 (2021) 80–83, https://doi.org/10.1016/j.mporth.2021.01.003.
[5] A.F. Hassanabad, A.N. Zarzycki, K. Jeon, J.A. Dundas, V. Vasanthan, J.F. Deniset, P.W.M. Fedak, Prevention of post-operative adhesions: a comprehensive review of present and emerging strategies, Biomolecules 11 (7) (2021) 1027, https://doi.org/10.3390/biom110710277.
[6] W.J. Metsemakers, R. Kuehl, T.F. Moriarty, R.G. Richards, M.H.J. Verhofstad, O. Borens, S. Kates, M. Morgenstern, Infection after fracture fixation: current surgical and microbiological concepts, Injury 49 (3) (2018) 511–522, https://doi.org/10.1016/j.injury.2016.09.019.
[7] R. Bogie, J.J. Arts, S.N. Koole, L.W. Van Rhijn, P.C. Willems, The use of metal sublaminar wires in modern growth-guidance scoliosis surgery: a report of 4 cases and literature review, Int. J. Spine Surg. 14 (2) (2020) 182–188, https://doi.org/10.14444/7017.
[8] H. Li, J. Lou, H. Liu, Migration of titanium cable into spinal cord and spontaneous C2 and C3 fusion: case report of possible causes of fatigue failure after posterior atlantoaxial fixation, Medicine (Baltimore) 95 (52) (2016) e5744, https://doi.org/10.1097/md.0000000000005744.
[9] J.S. Hayes, U. Seidenglanz, A.I. Pearce, S.G. Pearce, C.W. Archer, R.G. Richards, Surface polishing positively influences ease of plate and screw removal, eCM 19 (2010) 117–126, https://doi.org/10.22203/ecm.v019a12.
[10] J.S. Hayes, R.G. Richards, Surfaces to control tissue adhesion for osteosynthesis with metal implants: in vitro and in vivo studies to bring solutions to the patient, Expert Rev. Med. Devices 7 (1) (2010) 131–142, https://doi.org/10.1586/erd.09.55.
[11] V. Fröjd, P. Linderbäck, A. Wennerberg, L. Chávez de Paz, G. Svensäter, J. R. Davies, Effect of nanoporous TiO2 coating and anodized Ca2+ modification of titanium surfaces on early microbial biofilm formation, BMC Oral Health 11 (1) (2011), https://doi.org/10.1186/1472-6831-11-8.
[12] A. Al-Ahmad, M. Wiedmann-Al-Ahmad, A. Fackler, M. Follo, E. Hellwig, M. Bächle, C. Hannig, J.-S. Han, M. Wolkewitz, R. Kohal, In vivo study of the initial bacterial adhesion on different implant materials, Arch. Oral Biol. 58 (9) (2013) 1139–1147, https://doi.org/10.1016/j.archoralbio.2013.04.011.
[13] I. Furtat, M. Lupatsii, T. Murlanova, P. Vakuliuk, A. Gaidai, O. Biliayeva, H. Sobczuk, A. Golub, Nanocomposites with ornidazole—antibacterial and antiadhesive agents against gram-positive and gram-negative bacteria, Appl. Nanosci. 10 (8) (2020) 3193–3203, https://doi.org/10.1007/s13204-020-01260-x.
[14] N.E. Muzzio, M.A. Pasquale, E. Diamanti, D. Gregurec, M.M. Moro, O. Azzaroni, S. E. Moya, Enhanced antiadhesive properties of chitosan/hyaluronic acid polyelectrolyte multilayers driven by thermal annealing: low adherence for mammalian cells and selective decrease in adhesion for gram-positive bacteria, Mater. Sci. Eng. C Mater. Biol. Appl. 80 (2017) 677–687, https://doi.org/10.1016/j.msec.2017.07.016.
[15] F. Gamna, A. Cochis, A.C. Scalia, A. Vitale, S. Ferraris, L. Rimondini, S. Spriano, The use of vitamin E as an anti-adhesive coating for cells and bacteria for temporary bone implants, Surf. Coat. Technol. 444 (128694) (2022) 128694, https://doi.org/10.1016/j.surfcoat.2022.128694.
[16] S. Ferraris, S. Perero, P. Costa, G. Gautier di Confiengo, A. Cochis, L. Rimondini, F. Renaux, E. Vernè, M. Ferraris, S. Spriano, Antibacterial inorganic coatings on metallic surfaces for temporary fixation devices, Appl. Surf. Sci. 508 (144707) (2020) 144707, https://doi.org/10.1016/j.apsusc.2019.144707.
[17] T.C. Dakal, A. Kumar, R.S. Majumdar, V. Yadav, Mechanistic basis of antimicrobial actions of silver nanoparticles, Front. Microbiol. 7 (2016), https://doi.org/10.3389/fmicb.2016.01831.
[18] M. Cazzola, J. Barberi, S. Ferraris, A. Cochis, G. Cempura, A. Czyrska-Filemonowicz, L. Rimondini, S. Spriano, Bioactive titanium surfaces enriched with silver nanoparticles through an in situ reduction: looking for a balance between cytocompatibility and antibacterial activity, Adv. Eng. Mater. 25 (2) (2023), https://doi.org/10.1002/adem.202200883.
[19] Standard test methods for rating adhesion by tape test, Astm.org. https://www.astm.org/d3359-23.html. (Accessed 23 October 2024).
[20] J.J. Harrison, C.A. Stremick, R.J. Turner, N.D. Allan, M.E. Olson, H. Ceri, Microtiter susceptibility testing of microbes growing on peg lids: a miniaturized biofilm model for high-throughput screening, Nat. Protoc. 5 (7) (2010) 1236–1254, https://doi.org/10.1038/nprot.2010.71.
[21] A.M. Bolger, M. Lohse, B. Usadel, Trimmomatic: a flexible trimmer for Illumina sequence data, Bioinformatics 30 (15) (2014) 2114–2120, https://doi.org/10.1093/bioinformatics/btu170.
[22] B. Li, C.N. Dewey, RSEM: accurate transcript quantification from RNA-Seq data with or without a reference genome, BMC Bioinformatics 12 (1) (2011), https://doi.org/10.1186/1471-2105-12-323.
[23] A. Dobin, C.A. Davis, F. Schlesinger, J. Drenkow, C. Zaleski, S. Jha, P. Batut, M. Chaisson, T.R. Gingeras, STAR: ultrafast universal RNA-Seq aligner, Bioinformatics 29 (1) (2013) 15–21, https://doi.org/10.1093/bioinformatics/bts635.
[24] M.I. Love, W. Huber, S. Anders, Moderated estimation of fold change and dispersion for RNA-Seq data with DESeq2, Genome Biol. 15 (12) (2014) 550, https://doi.org/10.1186/s13059-014-0550-8.
[25] H. Heberle, G.V. Meirelles, F.R. da Silva, G.P. Telles, R. Minghim, InteractiVenn: a web-based tool for the analysis of sets through Venn diagrams, BMC Bioinformatics 16 (1) (2015), https://doi.org/10.1186/s12859-015-0611-3.
[26] M. Catauro, F. Barrino, M. Bononi, E. Colombini, R. Giovanardi, P. Veronesi, E. Tranquillo, Coating of titanium substrates with ZrO2 and ZrO2-SiO2 composites by sol-gel synthesis for biomedical applications: structural characterization, mechanical and corrosive behavior, Coatings 9 (3) (2019) 200, https://doi.org/10.3390/coatings9030200.
[27] S. Ferraris, S. Yamaguchi, N. Barbani, C. Cristallini, G. Gautier di Confiengo, J. Barberi, M. Cazzola, M. Miola, E. Vernè, S. Spriano, The mechanical and chemical stability of the interfaces in bioactive materials: the substrate-bioactive surface layer and hydroxyapatite-bioactive surface layer interfaces, Mater. Sci. Eng. C 116 (2020) 111238.
[28] S. Ferraris, A. Bobbio, M. Miola, S. Spriano, Micro- and nano-textured, hydrophilic and bioactive titanium dental implants, Surface and Coatings Technology 276 (2015) 374–383.
[29] M. Quirynen, C.M. Bollen, W. Papaioannou, J. Van Eldere, D. van Steenberghe, The influence of titanium abutment surface roughness on plaque accumulation and

gingivitis: short-term observations, Int. J. Oral Maxillofac. Implants 11 (2) (1996) 169–178.
[30] F. Heidenau, W. Mittelmeier, R. Detsch, M. Haenle, F. Stenzel, G. Ziegler, H. Gollwitzer, A novel antibacterial titania coating: metal ion toxicity and in vitro surface colonization, J. Mater. Sci. Mater. Med. 16 (10) (2005) 883–888, https://doi.org/10.1007/s10856-005-4422-3.
[31] The ZETA guide, Anton Paar. https://www.anton-paar.com/corp-en/the-zeta-guide/?srsltid=AfmBOopeLtcDuCbVl88K2wKwJ0cQpiDoPylWEXHz0SWcROVQrSV9eHVs. (Accessed 23 October 2024).
[32] B.S. Bal, M.N. Rahaman, Orthopedic applications of silicon nitride ceramics, Acta Biomater. 8 (8) (2012) 2889–2898, https://doi.org/10.1016/j.actbio.2012.04.031.
[33] S. Spriano, V. Sarath Chandra, A. Cochis, F. Uberti, L. Rimondini, E. Bertone, A. Vitale, C. Scolaro, M. Ferrari, F. Cirisano, G. Gautier di Confiengo, S. Ferraris, How do wettability, zeta potential and hydroxylation degree affect the biological response of biomaterials? Mater. Sci. Eng. C Mater. Biol. Appl. 74 (2017) 542–555, https://doi.org/10.1016/j.msec.2016.12.107.
[34] B. Gottenbos, D.W. Grijpma, H.C. van der Mei, J. Feijen, H.J. Busscher, Antimicrobial effects of positively charged surfaces on adhering gram-positive and gram-negative bacteria, J. Antimicrob. Chemother. 48 (1) (2001) 7–13, https://doi.org/10.1093/jac/48.1.7.
[35] Y. Alqahtani, L.E. Somerville, E.M. Vasarhelyi, J.L. Howard, B.A. Lanting, D.D. R. Naudie, S.J. MacDonald, R.W. McCalden, Minimum 2-year outcomes of a modern monoblock titanium fluted tapered revision stem for complex primary and revision total hip arthroplasty, J. Arthroplast. 39 (9S1) (2024) S208–S212, https://doi.org/10.1016/j.arth.2024.03.035.
[36] R. Sorrentino, A. Cochis, B. Azzimonti, C. Caravaca, J. Chevalier, M. Kuntz, A. A. Porporati, R.M. Streicher, L. Rimondini, Reduced bacterial adhesion on ceramics used for arthroplasty applications, J. Eur. Ceram. Soc. 38 (3) (2018) 963–970, https://doi.org/10.1016/j.jeurceramsoc.2017.10.008.
[37] A. Cochis, B. Azzimonti, C. Della Valle, E. De Giglio, N. Bloise, L. Visai, S. Cometa, L. Rimondini, R. Chiesa, The effect of silver or gallium doped titanium against the multidrug resistant Acinetobacter baumannii, Biomaterials 80 (2015) 80–95, https://doi.org/10.1016/j.biomaterials.2015.11.042.
[38] Ayse Kaplan, Hatice Mehtap Kutlu, Investigation of Silver Nitrate on Cytotoxicity and Apoptosis in MCF7 Human Breast Carcinoma Cells. Asian Pac. J. Cancer Biol., 5 (2), 49-56.
[39] L. Li, Z. Bi, Y. Hu, L. Sun, Y. Song, S. Chen, F. Mo, J. Yang, Y. Wei, X. Wei, Silver nanoparticles and silver ions cause inflammatory response through induction of cell necrosis and the release of mitochondria in vivo and in vitro, Cell Biol. Toxicol. 37 (2) (2020) 177–191, https://doi.org/10.1007/s10565-020-09526-4.
[40] M.E. Martin, D.K. Reaves, B. Jeffcoat, J.R. Enders, L.M. Costantini, S.T. Yeyeodu, D. Botta, T.J. Kavanagh, J.M. Fleming, Silver nanoparticles alter epithelial basement membrane integrity, cell adhesion molecule expression, and TGF-B1 secretion, Nanomedicine 21 (2019) 102070, https://doi.org/10.1016/j.nano.2019.102070.
[41] C. Frantz, K.M. Stewart, V.M. Weaver, The extracellular matrix at a glance, J. Cell Sci. 123 (24) (2010) 4195–4200, https://doi.org/10.1242/jcs.023820.
[42] M. Morais, A.L. Teixeira, F. Dias, V. Machado, R. Medeiros, J.A.V. Prior, Cytotoxic effect of silver nanoparticles synthesized by green methods in cancer, J. Med. Chem. 63 (23) (2020) 14308–14335, https://doi.org/10.1021/acs.jmedchem.0c01055.
[43] S. Dehghanizade, J. Arasteh, A. Mirzaie, Green synthesis of silver nanoparticles using Anthemis atropatana extract: characterization and in vitro biological activities, Artif. Cells Nanomed. Biotechnol. 46 (1) (2017) 160–168, https://doi.org/10.1080/21691401.2017.1304402.
[44] A. Kaler, S. Jain, U.C. Banerjee, Green and rapid synthesis of anticancerous silver nanoparticles by Saccharomyces boulardii and insight into mechanism of nanoparticle synthesis, Biomed. Res. Int. 2013 (2013) 872940, https://doi.org/10.1155/2013/872940.
[45] A. Szebeszczyk, J. Słowik, Heat shock proteins and metal ions - reaction or interaction? Comput. Struct. Biotechnol. J. 21 (2023) 3103–3108, https://doi.org/10.1016/j.csbj.2023.05.024.
[46] M.P. Mayer, B. Bukau, Hsp70 chaperones: cellular functions and molecular mechanism, Cell. Mol. Life Sci. 62 (6) (2005) 670–684, https://doi.org/10.1007/s00018-004-4464-6.
[47] S. Chakraborty, D. Chaudhuri, S. Banerjee, M. Bhatt, S. Haldar, Direct observation of chaperone-modulated talin mechanics with single-molecule resolution, Commun. Biol. 5 (1) (2022) 307, https://doi.org/10.1038/s42003-022-03258-3.
[48] W.T. Arthur, N.K. Noren, K. Burridge, Regulation of Rho family GTPases by cell-cell and cell-matrix adhesion, Biol. Res. 35 (2) (2002) 239–246, https://doi.org/10.4067/s0716-97602002000200016.
[49] C. Albigès-Rizo, P. Frachet, M.R. Block, Down regulation of talin alters cell adhesion and the processing of the alpha 5 beta 1 integrin, J. Cell Sci. 108 (Pt 10) (1995) 3317–3329, https://doi.org/10.1242/jcs.108.10.3317.
[50] J. Liu, Y. Wang, W.I. Goh, H. Goh, M.A. Baird, S. Ruehland, S. Teo, N. Bate, D. R. Critchley, M.W. Davidson, P. Kanchanawong, Talin determines the nanoscale architecture of focal adhesions, Proc. Natl. Acad. Sci. USA 112 (35) (2015) E4864–E4873, https://doi.org/10.1073/pnas.1512025112.
[51] A. Sedlář, M. Trávníčková, P. Bojarová, M. Vlachová, K. Slámová, V. Křen, L. Bačáková, Interaction between galectin-3 and integrins mediates cell-matrix adhesion in endothelial cells and mesenchymal stem cells, Int. J. Mol. Sci. 22 (10) (2021), https://doi.org/10.3390/ijms22105144.
[52] C.M. Micheel, S.J. Nass, G.S. Omenn, Board on Health Care Services, Board on Health Sciences Policy, Institute of Medicine, Omics-based Clinical Discovery: Science, Technology, and Applications, National Academies Press, Washington, D. C., DC, 2012.
[53] S. Haider, R. Pal, Integrated analysis of transcriptomic and proteomic data, Curr. Genomics 14 (2) (2013) 91–110, https://doi.org/10.2174/1389202911314020003.
[54] I. González, K.-A.L. Cao, M.J. Davis, S. Déjean, Visualising associations between paired "omics" data sets, BioData Min. 5 (1) (2012) 19, https://doi.org/10.1186/1756-0381-5-19.
[55] J. Reimand, T. Arak, P. Adler, L. Kolberg, S. Reisberg, H. Peterson, J. Vilo, G: Profiler-a web server for functional interpretation of gene lists (2016 update), Nucleic Acids Res. 44 (W1) (2016) W83–W89, https://doi.org/10.1093/nar/gkw199.
[56] J. Reimand, R. Isserlin, V. Voisin, M. Kucera, C. Tannus-Lopes, A. Rostamianfar, L. Wadi, M. Meyer, J. Wong, C. Xu, D. Merico, G.D. Bader, Pathway enrichment analysis and visualization of omics data using g:Profiler, GSEA, Cytoscape and EnrichmentMap, Nat. Protoc. 14 (2) (2019) 482–517, https://doi.org/10.1038/s41596-018-0103-9.